Inorganic Chemistry

including bioinorganic chemistry

September 1, 2014
Volume 53, Number 17
pubs.acs.org/IC

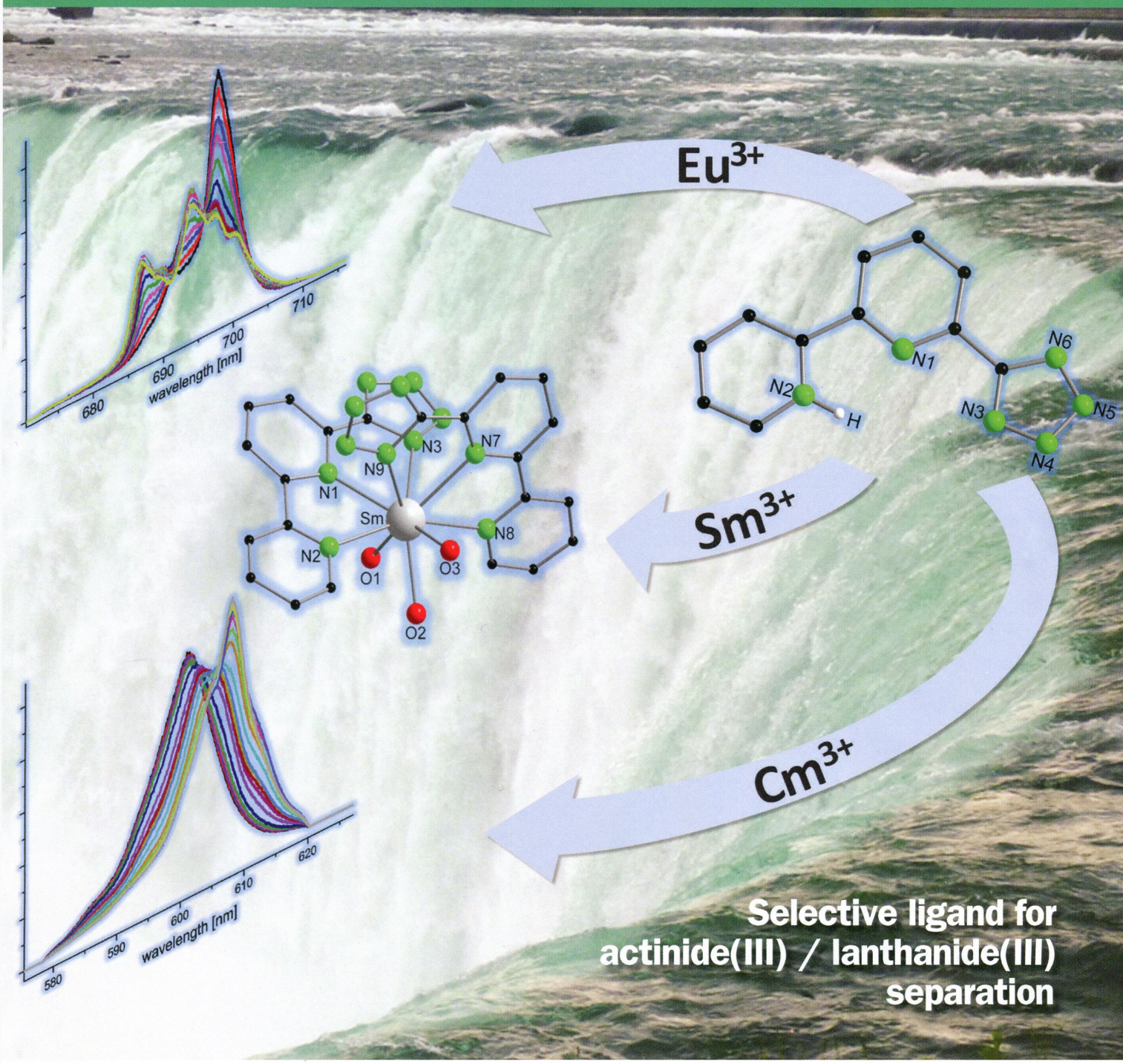

Selective ligand for actinide(III) / lanthanide(III) separation

Inorganic Chemistry

SEPTEMBER 1, 2014
VOLUME 53 ISSUE 17

INOCAJ 53(17) 8839–9440 (2014)
ISSN 0020-1669

ON THE COVER: The complexation of a tridentate nitrogen-donor ligand with elements from the trivalent lanthanide and actinide series was studied via X-ray crystallography and fluorescence emission spectroscopy, with examples shown for Eu^{III}, Sm^{III}, and Cm^{III}. See J. Kratsch, B. B. Beele, C. Koke, M. A. Denecke, A. Geist, P. J. Panak, and P. W. Roesky, p 8949.

Communications

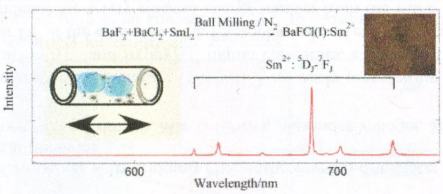

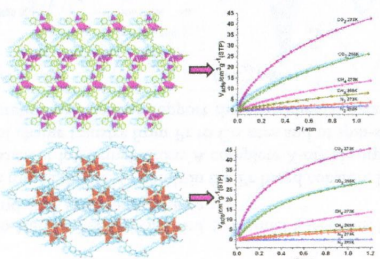

8845 S

dx.doi.org/10.1021/ic5011314

Synthesis and Characterization of Inorganic–Organic Hybrid Gallium Selenides

Sarah J. Ewing and Paz Vaqueiro*

The synthesis and characterization of two semiconducting hybrid gallium selenides, which consist of neutral inorganic layers covalently bonded to 1,2-diaminocyclohexane, are described.

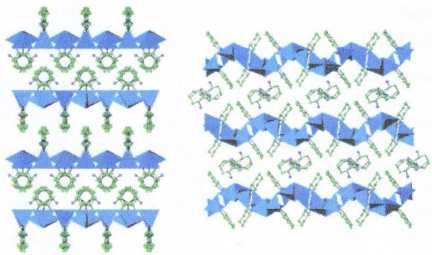

8848 S

dx.doi.org/10.1021/ic501120k

Dual-Channel-Mediated Spin Coupling for One-Electron-Oxidized Cobalt(II)-Saddled Porphyrin

Ru-Jen Cheng,* Yu-Hsuan Chen, Ching-Chin Chen, Gene-Hsiang Lee, Shie-Ming Peng, and Peter Ping-Yu Chen*

A dual channel composed by an axial ligand (X) and a para substituent (R) in phenyl fragments of $[Co^{II}[OET(p\text{-}R)PP]]^{+}X^{-}$ mediated antiferromagnetic coupling between d_{z^2} and a_{2u} spins to cause a change of the magnetic property from diamagnetism to paramagnetism. As the axial ligand X = I and R = CF_3, the strongest spin coupling will be induced, and paramagnetic characters are readily tuned up by other combinations of X and R.

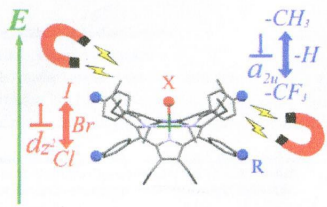

8851 S

dx.doi.org/10.1021/ic5015972

Partial Hydrogenation of a Tetranuclear Titanium Nitrido Complex with Ammonia Borane

Jorge Caballo, Mariano González-Moreiras, Maider Greño, Miguel Mena, Adrián Pérez-Redondo, and Carlos Yélamos*

Hydrogenation of $[\{Ti(\eta^5\text{-}C_5Me_5)\}_4(\mu_3\text{-}N)_4]$ with NH_3BH_3 leads to the paramagnetic imidonitrido complex $[\{Ti(\eta^5\text{-}C_5Me_5)\}_4(\mu_3\text{-}N)_3(\mu_3\text{-}NH)]$, which can also be obtained through stepwise protonation at one nitrido ligand and one-electron reduction of a titanium atom.

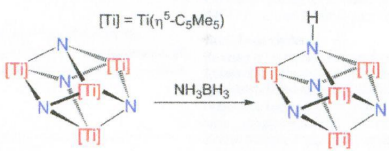

Articles

8854 dx.doi.org/10.1021/ic403117j

Stability of the Cationic Oxidation States in $Pr_{0.50}Sr_{0.50}CoO_3$ across the Magnetostructural Transition by X-ray Absorption Spectroscopy

Jessica Padilla-Pantoja,* Javier Herrero-Martín, Pierluigi Gargiani, S. Manuel Valvidares, Vera Cuartero, Kurt Kummer, Oliver Watson, Nicholas B. Brookes, and José Luis García-Muñoz

The stability of the Pr valence and the role of the Pr−O bonds in the Pr-based cobaltite $Pr_{0.50}Sr_{0.50}CoO_3$ across the unexpected magnetostructural transition were studied at low temperature. A complete X-ray absorption spectroscopy study as a function of temperature revealed the absence of charge transfer from Pr to Co sites and of spin-state transitions in the Co ions despite the strong Pr−O hybridization. Theoretical calculations support the experimental data.

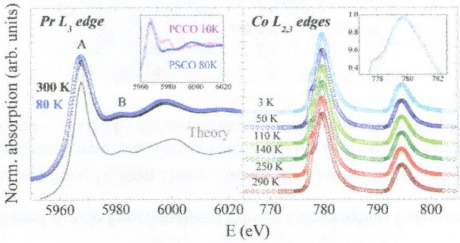

8859 S dx.doi.org/10.1021/ic4031206

Dinuclear Ru/Ni, Ir/Ni, and Ir/Pt Complexes with Bridging Phenanthroline-5,6-dithiolate: Synthesis, Structure, and Electrochemical and Photophysical Behavior

David Schallenberg, Antje Neubauer,* Elisa Erdmann, Marco Tänzler, Alexander Villinger, Stefan Lochbrunner, and Wolfram W. Seidel*

Dinuclear complexes with phenanthroline-5,6-dithiolate ($phendt^{2-}$) are easily prepared by a consecutive coordination and protective group strategy. For $[Ru(bpy)_2]^{2+}$ and $Ir(ppy)_2]^+$ diimin complexes, a significant photoluminescence quenching is observed by coordination of Ni^{II} or Pt^{II} at the dithiolato unit. Photophysical and electrochemical investigations in combination with DFT calculations provide evidence for a very efficient energy transfer from the Ru/Ir to the Ni complex moiety with a rate constant $k > 5 \times 10^9\ s^{-1}$.

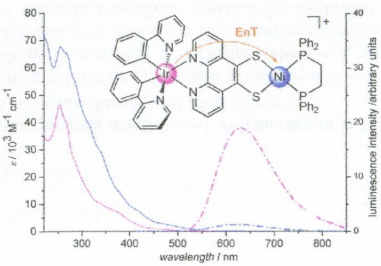

8874 (S) dx.doi.org/10.1021/ic500272b

Structure and Conformation of the Medium-Sized Chlorophosphazene Rings

David J. Bowers, Brian D. Wright, Vincenzo Scionti, Anthony Schultz, Matthew J. Panzner, Eric B. Twum, Lin-Lin Li, Bryan C. Katzenmeyer, Benjamin S. Thome, Peter L. Rinaldi, Chrys Wesdemiotis, Wiley J. Youngs, and Claire A. Tessier*

The cyclic phosphazenes $[PCl_2N]_m$ (with m = 5–9) have been isolated. They have been characterized by ESI-MS, ^{31}P NMR spectroscopy, and X-ray crystallography (m = 5, 6, 8). The crystal structures of $[P(OPh)_2N]_7$ and $[P(OPh)_2N]_8$ are also reported. Comparisons among the solid-state structures of five octameric $[P(X)_2N]_8$ (X = Cl, OPh, OMe, NMe_2, Me) suggest that chlorophosphazenes should not be considered prototypical phosphazenes, because of the strong influence of halogen bonding.

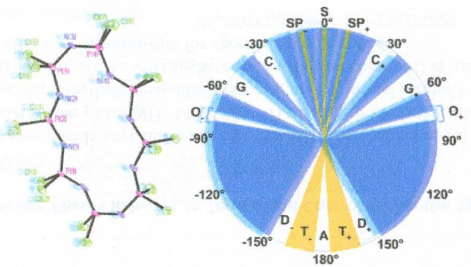

8887 (S) dx.doi.org/10.1021/ic500495a

Incorporation of Monovalent Cations in Sulfate Green Rust

B. C. Christiansen, K. Dideriksen, A. Katz, S. Nedel, N. Bovet, H. O. Sørensen,* C. Frandsen, C. Gundlach, M. P. Andersson, and S. L. S. Stipp

Green rust is a naturally occurring layered mixed-valent ferrous–ferric hydroxide, which can react with a range of redox-active compounds. We provide evidence that the interlayers of sulfate-bearing green rust also can incorporate the monovalent cations Na^+, K^+, Rb^+, and Cs^+, using X-ray photoelectron spectroscopy and synchrotron X-ray scattering. In addition, sequential washing of the materials with water showed that Na^+ and K^+ were fixed in the interlayer, whereas Rb^+ and Cs^+ could be removed.

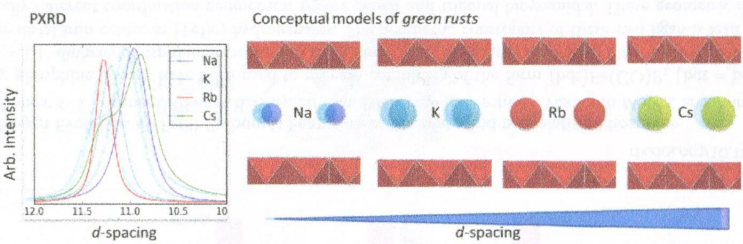

8895 S dx.doi.org/10.1021/ic500501r

Local Coordination Geometry Perturbed β-Diketone Dysprosium Single-Ion Magnets

Jing Zhu, Changzheng Wang, Fang Luan, Tianqi Liu, Pengfei Yan, and Guangming Li*

A series of three β-diketone (TIF) mononuclear dysprosium complexes with different coordination geometries on Dy(III) ions exhibit unqiue magnetic behaviors in which slow magnetic relaxations with a considerably high energy barrier (U_{eff}/k_B) of 57.9 K are observed.

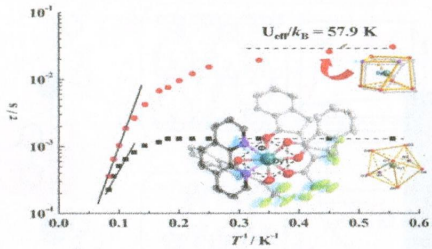

8902 S dx.doi.org/10.1021/ic500518a

Band Gap Engineering of ZnO using Core/Shell Morphology with Environmentally Benign Ag_2S Sensitizer for Efficient Light Harvesting and Enhanced Visible-Light Photocatalysis

Sunita Khanchandani, Pawan Kumar Srivastava, Sandeep Kumar, Subhasis Ghosh, and Ashok K. Ganguli*

Band gap engineering of ZnO nanorods was achieved by introducing a core/shell geometry with the environmentally benign Ag_2S sensitizer as the shell. Sensitizing ZnO with Ag_2S resulted in substantially enhanced light absorption and photodegradation of MB under illumination of visible light, in comparison to Cd sensitizers, owing to the narrow band gap of Ag_2S, thus unraveling the superiority of Ag_2S as an efficient sensitizer to sensitize wide band gap semiconductors and the potential to supersede Cd-based sensitizers for eco-friendly applications.

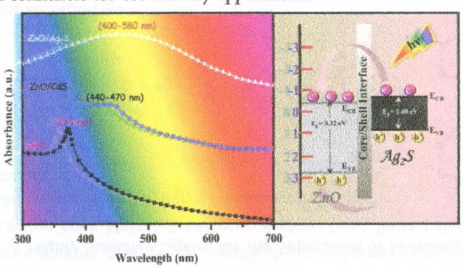

8913 (S) dx.doi.org/10.1021/ic500554z

Structural Phase Transitions of a Layered Organic–Inorganic Hybrid Compound: Tetra(cyclopentylammonium) Decachlorotricadmate(II), $[C_5H_9NH_3]_4Cd_3Cl_{10}$

Wei-Qiang Liao, Guang-Quan Mei,* Heng-Yun Ye, Ying-Xuan Mei, and Yi Zhang*

A layered organic–inorganic hybrid compound, tetra(cyclopentylammonium) decachlorotricadmate(II), undergoes two structural phase transitions, at 197.3 (T_1) and 321.6 (T_2) K. The phase transition at 197.3 K is triggered by the order–disorder transition of the cyclopentylammonium cations, while the phase transition at 321.6 K is due to the distortion of the two-dimensional $[Cd_3Cl_{10}]^{4-}{}_n$ network.

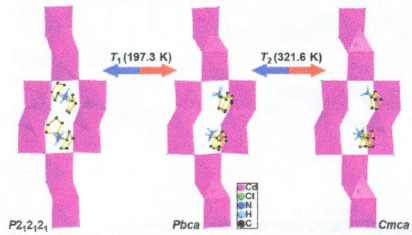

8919 (S) dx.doi.org/10.1021/ic5012988

Catalytic Hydrogen Evolution by Fe(II) Carbonyls Featuring a Dithiolate and a Chelating Phosphine

Souvik Roy, Shobeir K. S. Mazinani, Thomas L. Groy, Lu Gan, Pilarisetty Tarakeshwar, Vladimiro Mujica, and Anne K. Jones*

Two chelating phosphine ligands have been used to prepare complexes of the form (bdt)Fe(CO)P_2 [bdt = benzene-1,2-dithiolate; P_2 = 1,1′-diphenylphosphinoferrocene (**1**) or methyl-2-{bis(diphenylphosphinomethyl)amino}acetate (**2**)] as models for the distal iron center in [FeFe]-hydrogenases. The geometric constraints of these two ligands lead to complexes with dramatically different coordination geometries: square planar and trigonal bipyramidal. These geometric differences are reflected in different reactivities toward protons and CO.

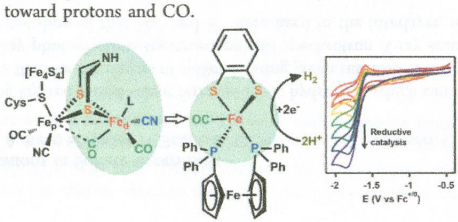

8930 (S) dx.doi.org/10.1021/ic5006659

Preferential Solvation of Metastable Phases Relevant to Topological Control Within the Synthesis of Metal–Organic Frameworks

Xiaoning Yang* and Aurora E. Clark*

Combined density functional theory calculations and molecular dynamics simulations reveal the hydrophobic nature of a model cluster based upon the metastable phase NH_2-MOF-235(Al), causing preferential solvation of the cluster by hydrophobic cosolvents (acetonitrile, dimethylformamide, methanol, and isopropyl alcohol) in binary aqueous solutions. These observations are anticipated to impact the intermediate and final phases observed in metal–organic framework (MOF) synthesis by creating favorable solvation environments for specific MOF topologies.

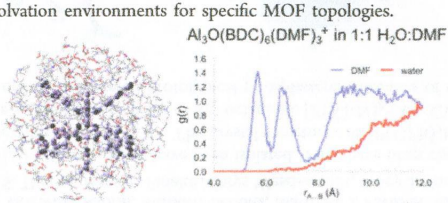

8941 S dx.doi.org/10.1021/ic5007346

$AgNb_7O_{18}$: An Ergodic Relaxor Ferroelectric

David I. Woodward* and Richard Beanland

$AgNb_7O_{18}$ is an ergodic relaxor ferroelectric at room temperature with an incipient transition to the nonergodic state. Electron diffraction confirms a locally polar symmetry, while X-ray diffraction perceives a nonpolar structure. All ions are repelled away from zones where NbO_6 octahedra are edge-sharing.

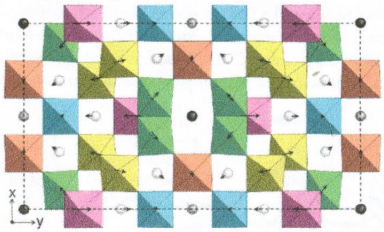

8949 S dx.doi.org/10.1021/ic5007549

6-(Tetrazol-5-yl)-2,2′-bipyridine: A Highly Selective Ligand for the Separation of Lanthanides(III) and Actinides(III)

Jochen Kratsch, Björn B. Beele, Carsten Koke, Melissa A. Denecke, Andreas Geist, Petra J. Panak,* and Peter W. Roesky*

The coordination properties of 6-(tetrazol-5-yl)-2,2′-bipyridine for actinide(III)/lanthanide(III) separations are examined.

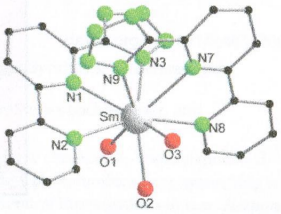

8959 S dx.doi.org/10.1021/ic500810d

Ab Initio Chemical Synthesis of Designer Metal Phosphate Frameworks at Ambient Conditions

Alok Ch. Kalita, Nayanmoni Gogoi, Ritambhara Jangir, Subramaniam Kuppuswamy, Mrinalini G. Walawalkar, and Ramaswamy Murugavel*

The pandemonium surrounding the synthesis of porous metal phosphate frameworks has been addressed by a rational soft chemical route. A molecular zinc phosphate precursor featuring a D4R core has been glued into hierarchical zinc phosphate frameworks through robust coordinate linkages.

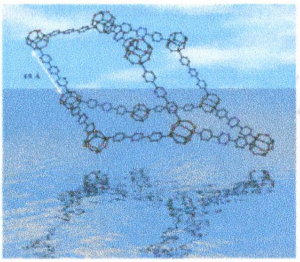

8970 S dx.doi.org/10.1021/ic500885r

Exchange Interactions at the Origin of Slow Relaxation of the Magnetization in $\{TbCu_3\}$ and $\{DyCu_3\}$ Single-Molecule Magnets

Fraser J. Kettles, Victoria A. Milway, Floriana Tuna, Rafael Valiente, Lynne H. Thomas, Wolfgang Wernsdorfer, Stefan T. Ochsenbein,* and Mark Murrie*

We have determined the exchange interactions in new $\{TbCu_3\}$ and $\{DyCu_3\}$ SMMs, with inelastic neutron scattering (INS) spectroscopy. We found that the fundamental INS excitations correspond to Cu^{II} spin flips. These have energies similar to the thermodynamic barriers for magnetization reversal, which we determined using ac magnetic susceptibility measurements. This indicates the importance of these spin flips for the magnetic relaxation and therefore the importance of the 3d−4f exchange interactions for the thermodynamic energy barrier.

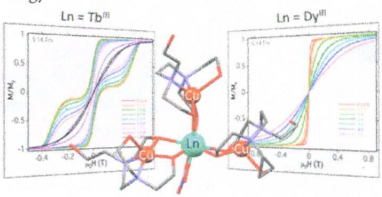

8979 S dx.doi.org/10.1021/ic500902q

Three-Dimensionality of Electronic Structures and Thermoelectric Transport in $SrZrN_2$ and $SrHfN_2$ Layered Complex Metal Nitrides

Isao Ohkubo* and Takao Mori

Layered materials have several properties that make them suitable as high-performance thermoelectric materials. In this study, we focus on the layered complex metal nitrides $SrMN_2$ (M = Zr, Hf). The electronic structures and thermoelectric properties for $SrMN_2$ were calculated using density-functional theory and Boltzmann theory, respectively. Despite the layered structure, $SrMN_2$ had three-dimensional electronic structures and isotropic electronic transport, indicating the appearance of large Seebeck coefficients and large electronic thermoelectric figures of merit.

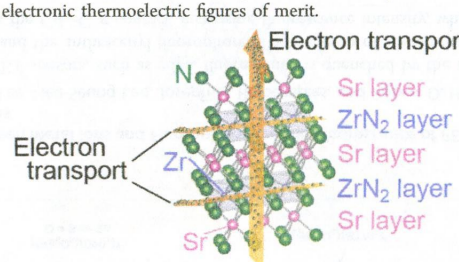

8985 S dx.doi.org/10.1021/ic500905z

Targeted Structure Modulation of "Pillar-Layered" Metal–Organic Frameworks for CO_2 Capture

Zhi-Hong Xuan, Da-Shuai Zhang, Ze Chang,* Tong-Liang Hu, and Xian-He Bu*

Two zinc MOFs with similar "pillar-layered" framework structures have been synthesized and investigated with their CO_2 adsorption properties. The results reveal that the structure factors (pore dimension and flexibility) as well as the binding affinity could determine the CO_2 capture ability of MOFs.

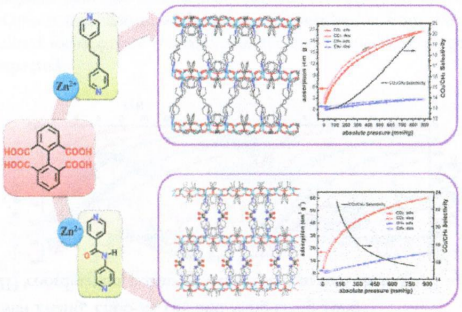

8991 S dx.doi.org/10.1021/ic5009126

An Al/P-Based Frustrated Lewis Pair as an Efficient Ambiphilic Ligand: Coordination of Boron Trihalides, Rearrangement, and Formation of HBX_2 Complexes (X = Br, I)

Werner Uhl,* Christian Appelt, Agnes Wollschläger, Alexander Hepp, and Ernst-Ulrich Würthwein

The coordination of ambiphilic boron trihalides by an Al/P-based frustrated Lewis pair is reported. Spontaneous rearrangement reactions and β-hydride elimination afforded adducts of unstable HBX_2 (X = Br, I) molecules via the intermediate formation of a borenium cation.

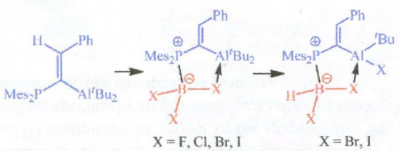

9000 S dx.doi.org/10.1021/ic500919e

Potassium–Sulfur Batteries: A New Member of Room-Temperature Rechargeable Metal–Sulfur Batteries

Qing Zhao, Yuxiang Hu, Kai Zhang, and Jun Chen*

Room-temperature potassium–sulfur (K-S) batteries were assembled using ordered mesoporous carbon (CMK-3)/sulfur and polyanilime (PANI) coated CMK-3/sulfur composites as the cathode and metallic potassium as the anode. The CMK-3/sulfur composite with 40.8 wt % S displays a discharge capacity of 512.7 mAh g^{-1} with K_2S_3 as the major discharge product that can recur to sulfur after the following charge. A coating of conductive polyanilime (PANI) on the CMK-3/sulfur composite is effective in enhancing the cycling performance.

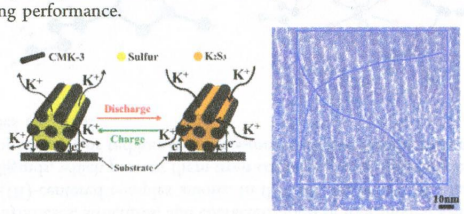

9006 S dx.doi.org/10.1021/ic500553v

The First Water-Soluble Hexarhenium Cluster Complexes with a Heterocyclic Ligand Environment: Synthesis, Luminescence, and Biological Properties

Michael A. Shestopalov, Kristina E. Zubareva, Olga P. Khripko, Yuri I. Khripko, Anastasiya O. Solovieva, Natalia V. Kuratieva, Yuri V. Mironov, Noboru Kitamura, Vladimir E. Fedorov, and Konstantin A. Brylev*

The new water-soluble cluster complexes $[\{Re_6(\mu_3\text{-}Q)_8\}(BTA)_6]^{4-}$ (Q = S, Se; BTA = benzotriazolate ion) possessing photoluminescence with relatively high lifetime and quantum yield values were found to be promising as bioimaging agents: they were taken up by the cells illuminating them under UV irradiation and, at the same time, did not exhibit acute cytotoxic effects at the concentration level of practical biological applications.

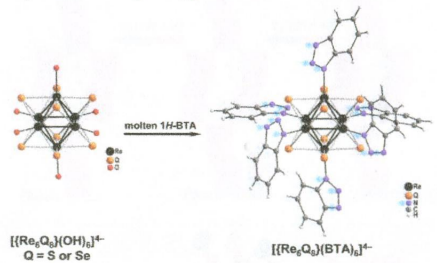

9014 S dx.doi.org/10.1021/ic5008632

The Effect of π Contacts between Metal Ions and Fluorophores on the Fluorescence of PET Sensors: Implications for Sensor Design for Cations and Anions

Joseph W. Nugent, Hyunjung Lee, Hee-Seung Lee, Joseph H. Reibenspies, and Robert D. Hancock*

The idea is explored that in PET sensors, such as adpa, fluorescence is quenched by the formation of π contacts between diamagnetic heavy metal ions and the anthracenyl fluorophore. The addition of anions that coordinate to the Cd(II) in the Cd(II)/adpa complex weakens the Cd···C π contact, increasing fluorescence intensity, which suggests a new type of anion sensor.

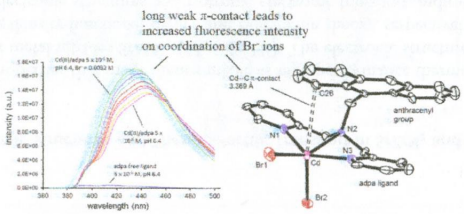

9027 S dx.doi.org/10.1021/ic500979p

Highly Luminescent Salts Containing Well-Shielded Lanthanide-Centered Complex Anions and Bulky Imidazolium Countercations

Si-Fu Tang,* Chantal Lorbeer, Xinjiao Wang, Pushpal Ghosh, and Anja-Verena Mudring*

In this paper, we report on the syntheses, structures, and characterization of four molten salts containing imidazolium cations and europium(III)- or terbium(III)-centered complex anions. In the complex anions, the lanthanide centers are wrapped by four pseudodiketonate anionic ligands, which prevent them from contacting with high-frequency oscillators and allow them to show intense characteristic europium(III) or terbium(III) emission, small line widths, high color purity, high quantum yields (30–49%), and long decay times (>2 ms).

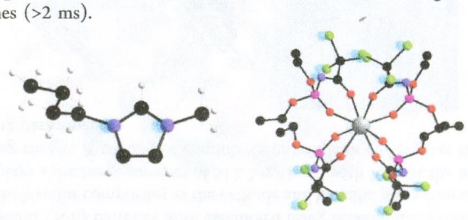

9036 S dx.doi.org/10.1021/ic5009945

Dinuclear Zinc(II) Complexes with Hydrogen Bond Donors as Structural and Functional Phosphatase Models

Simone Bosch, Peter Comba,* Lawrence R. Gahan, and Gerhard Schenk

The type and arrangement of substituents in the dinucleating ligand strongly modify the structure of the corresponding dizinc(II) complexes, as shown in the graphic, and this is indicated to be due to hydrogen bonding, specifically to substrate and inhibitor molecules. This allows the understanding and optimization of the phosphatase activity.

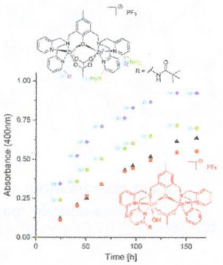

9052 S dx.doi.org/10.1021/ic501013x

Gadolinium Oxalate Derivatives with Enhanced Magnetocaloric Effect via Ionothermal Synthesis

Yan Meng, Yan-Cong Chen, Ze-Min Zhang, Zhuo-Jia Lin, and Ming-Liang Tong*

Two new oxalate-bridged Gd(III) coordination polymers were tested to find their MCE values.

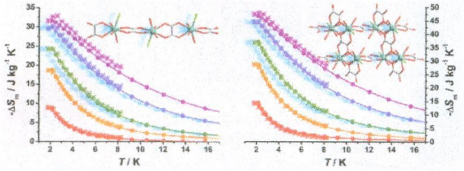

9058 S dx.doi.org/10.1021/ic501068e

$LnV_3Te_3O_{15}(OH)_3{\cdot}nH_2O$ (Ln = Ce, Pr, Nd, Sm, Eu, Gd; n = 1−2): A New Series of Semiconductors with Mixed-Valent Tellurium (IV,VI) Oxoanions

Jian Lin, Kariem Diefenbach, Jingcheng Fu, Justin N. Cross, Ronald J. Clark, and Thomas E. Albrecht-Schmitt*

$LnV_3Te_3O_{15}(OH)_3{\cdot}nH_2O$ (Ln = Ce, Pr, Nd, Sm, Eu, Gd) have been prepared, their structures elucidated, and physical property measurements carried out. These compounds adopt a three-dimensional (3D) channel structure. Two types of oxoanions, $Te^{IV}O_3^{2-}$ trigonal pyramids and $Te^{VI}O_6^{6-}$ octahedra, coexist in these compounds. A clear increase in the strength of short-range antiferromagnetic correlations was found with the shortening of distances between magnetically coupled Ln^{3+} ions.

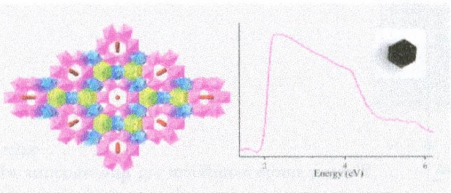

9065 S dx.doi.org/10.1021/ic501091g

High-Temperature, High-Pressure Hydrothermal Synthesis, Characterization, and Structural Relationships of Layered Uranyl Arsenates

Hsin-Kuan Liu, Eswaran Ramachandran, Yi-Hsin Chen, Wen-Jung Chang, and Kwang-Hwa Lii*

Five new uranyl arsenates were synthesized under hydrothermal conditions at about 560 °C and 1440 bar and structurally characterized by single-crystal X-ray diffraction. The five compounds have layer structures consisting of uranyl square, pentagonal, and hexagonal bipyramids as well as AsO_4 tetrahedra. Two of the structures can be obtained by splitting the β-U_3O_8-type sheet into complex chains and connecting the chains by arsenates.

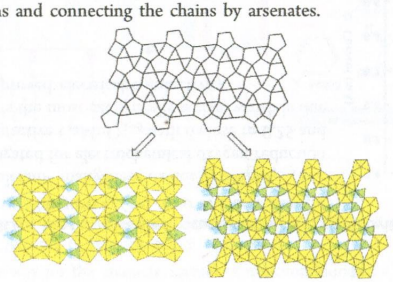

9073 S dx.doi.org/10.1021/ic501092k

Synthesis of Novel Two-Phase Co@SiO_2 Nanorattles with High Catalytic Activity

Nan Yan, Ziang Zhao, Yan Li, Fang Wang, Hao Zhong, and Qianwang Chen*

Co@SiO_2 nanorattles as a mixture of hcp-Co and fcc-Co phases have been designed and prepared as a substitute for noble metal catalysts. The nanorattles exhibit both superior catalytic activity and high stability for the reduction of p-nitrophenol, which suggests the catalytic ability could be enhanced by making phase junctions in a single material.

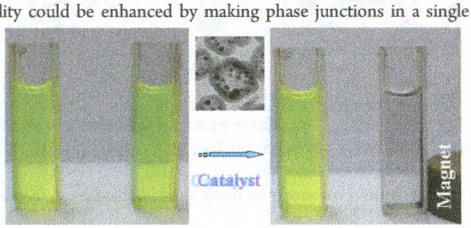

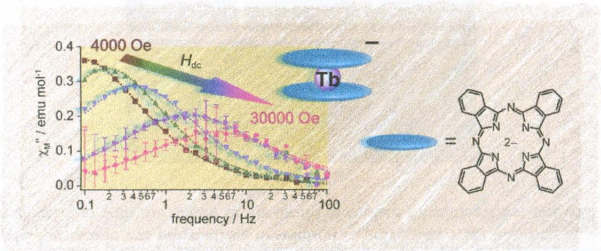

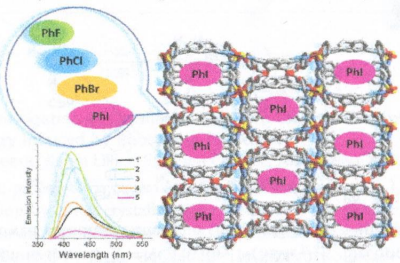

9095 S dx.doi.org/10.1021/ic501117f

Metallodithiolates as Ligands to Dinitrosyl Iron Complexes: Toward the Understanding of Structures, Equilibria, and Spin Coupling

Tiffany A. Pinder, Steven K. Montalvo, Chung-Hung Hsieh, Allen M. Lunsford, Ryan D. Bethel, Brad S. Pierce, and Marcetta Y. Darensbourg*

The N_2S_2 tight binding site for nickel in the acetyl coA enzyme active site serves as inspiration for development of MN_2S_2 complexes as S-donor ligands to dia- and paramagnetic metal acceptors.

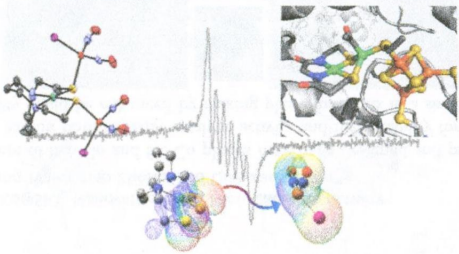

9106 S dx.doi.org/10.1021/ic501631h

Nonstoichiometric Perovskite $CaMnO_{3-\delta}$ for Oxygen Electrocatalysis with High Activity

Jing Du, Tianran Zhang, Fangyi Cheng, Wangsheng Chu, Ziyu Wu, and Jun Chen*

Nonstoichiometric perovskite-type calcium−manganese oxides ($CaMnO_{3-\delta}$, $0 < \delta \leq 0.5$) were synthesized and investigated for electrochemical oxygen reduction and oxygen evolution. The oxygen-defective $CaMnO_{3-\delta}$ with δ close to 0.25 and average Mn valence near ~3.5 exhibits the most catalytically active, which is due to favored oxygen activation and improved electrical conductivity.

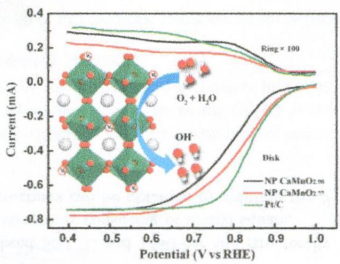

9115 S dx.doi.org/10.1021/ic501088t

New Kagome Metal $Sc_3Mn_3Al_7Si_5$ and Its Gallium-Doped Analogues: Synthesis, Crystal Structure, and Physical Properties

Hua He,* Wojciech Miiller, and Meigan C. Aronson

A new intermetallic compound, $Sc_3Mn_3Al_7Si_5$, has been synthesized from flux method. It crystallizes with the $Sc_3Ni_{11}Si_4$-type structure with the manganese atoms forming geometrically frustrated Kagome nets.

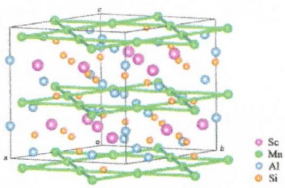

9122 dx.doi.org/10.1021/ic501136m

Halide-Bridged Binuclear HX-Splitting Catalysts

David C. Powers, Seung Jun Hwang, Shao-Liang Zheng, and Daniel G. Nocera*

Photochemical energy conversion via closed HX-splitting schemes requires both reduction of protons to H_2 and oxidation of halides to X_2 to be accomplished. Halide-bridged structures have been proposed as critical intermediates in the halide oxidation half-reaction of HX splitting catalyzed by Rh_2 complexes. Accordingly, a new family of chloride-bridged photocatalysts has been developed, and the resulting photocatalysts are more efficient for H_2 evolution than their related unbridged congeners.

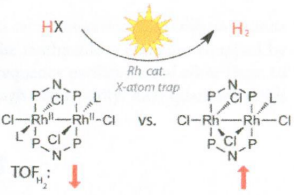

9129 dx.doi.org/10.1021/ic501149u

Anomalous One-Electron Processes in the Chemistry of Uranium Nitrogen Multiple Bonds

Kimberly C. Mullane, Andrew J. Lewis, Haolin Yin, Patrick J. Carroll, and Eric J. Schelter*

The synthesis of a uranium(V) trityl imido complex: $U^{V}(=NCPh_3)[N(SiMe_3)_2]_3$ proceeded through an anomalous series of one-electron steps from the reaction of $U^{III}[N(SiMe_3)_2]_3$ and Ph_3CN_3, in contrast with the conventional two-electron chemistry observed in the synthesis of $U^{V}(=NSiMe_3)[N(SiMe_3)_2]_3$. Further oxidation of $U^{V}(=NCPh_3)[N(SiMe_3)_2]_3$ resulted in sterically induced reduction to form $U^{VI}(=NCPh_3)Br_2[N(SiMe_3)_2]_2$. Electrochemical and computational analyses of these and related compounds showed substituent effects in the chemistry of uranium−nitrogen multiple bonds.

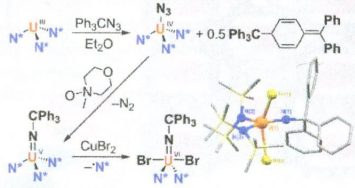

9140 dx.doi.org/10.1021/ic501164c

Zirconium Complexes of Phenylene-Bridged {ONSO} Ligands: Coordination Chemistry and Stereoselective Polymerization of *rac*-Lactide

Ayellet Stopper, Konstantin Press, Jun Okuda, Israel Goldberg, and Moshe Kol*

The coordination chemistry and lactide polymerization catalysis of zirconium complexes of the new phenylene-bridged thio-imine diphenolate ligands are described. The $[\{ONSO\}Zr(O^tBu)_2]$ complexes were fluxional with the ligands unexpectedly wrapping in a *fac-fac* mode. *Rac*-lactide was polymerized in solution to poly(lactic acid) featuring tacticity which ranged from heterotactic to atactic in correlation with the nature of the ligand phenolate substituents but not with the degree of complex fluxionality.

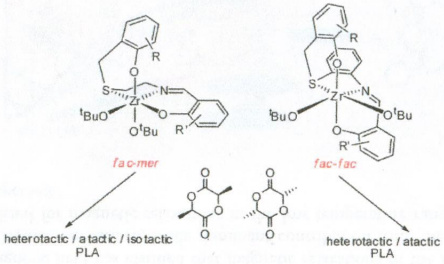

9151 S dx.doi.org/10.1021/ic501129y

Reversibly Tunable Upconversion Luminescence by Host–Guest Chemistry

Takaaki Taniguchi,* Tomoaki Murakami, Asami Funatsu, Kazuto Hatakeyama, Michio Koinuma, and Yasumichi Matsumoto

Highly tunable UPC luminescence was achieved through a host–guest chemistry approach. Interlayer ion exchange reactions reversibly tuned the emission intensity and green-red color of Er/Yb-codoped $A_2La_2Ti_3O_{10}$ layered perovskite, where A corresponds to proton and alkali metal ions, enabling the visualization of host–guest interactions and reactions.

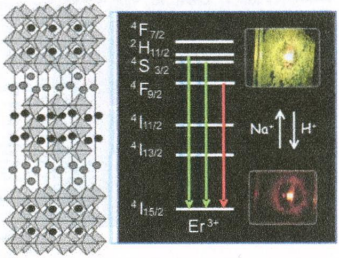

9156 S dx.doi.org/10.1021/ic5011924

Electronic Control of Ligand-Binding Preference of a Myoglobin Mutant

Ryu Nishimura, Daichi Matsumoto, Tomokazu Shibata, Sachiko Yanagisawa, Takashi Ogura, Hulin Tai, Takashi Matsuo, Shun Hirota, Saburo Neya, Akihiro Suzuki, and Yasuhiko Yamamoto*

The study demonstrated that the preferential binding of O_2 over CO by the L29F mutant protein was achieved through increasing ρ_{Fe}, and the ordinary ligand-binding preference, that is, the preferential binding of CO over O_2, by the protein through decreasing ρ_{Fe}. Thus, the O_2 and CO binding preferences of the L29F mutant protein were controlled through electronic modulation of intrinsic heme Fe reactivity through a change in ρ_{Fe}.

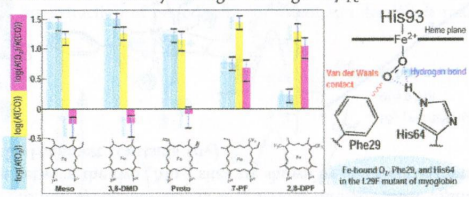

9166 S dx.doi.org/10.1021/ic501194n

New Approach for the Step by Step Control of Magnetic Nanostructure Functionalization

P. Riani, M. A. Lucchini,* S. Thea, M. Alloisio, G. Bertoni, and F. Canepa

This Article introduces an innovative way for the characterization of multifunctionalized magnetic nanoparticles. The method is used to control the synthesis of fluorescent magnetic nanostructures. Looking at the behavior in an oscillating magnetic field, we are able to follow the dimensional evolution of each intermediate; the results are confirmed with a second technique based on fluorescence. The method can be used in every functionalization involving a magnetic core regardless the nature of the external functionalization.

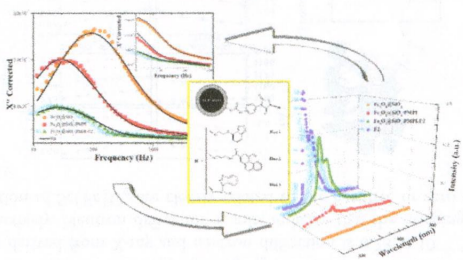

9174 (S) dx.doi.org/10.1021/ic501189n

Ordered Structure and Thermal Expansion in Tungsten Bronze $Pb_2K_{0.5}Li_{0.5}Nb_5O_{15}$

Kun Lin, Yangchun Rong, Hui Wu, Qingzhen Huang, Li You, Yang Ren, Longlong Fan, Jun Chen, and Xianran Xing*

When small Li^+ cations exist, the tetragonal tungsten bronze oxide $Pb_2K_{0.5}Li_{0.5}Nb_5O_{15}$ shows an ordered structural feature at room temperature. This compound exhibits a stronger negative thermal expansion behavior along the polar *b* axis compared with the parent $Pb_2KNb_5O_{15}$, which is associated with more Pb^{2+} in the large pentagonal caves.

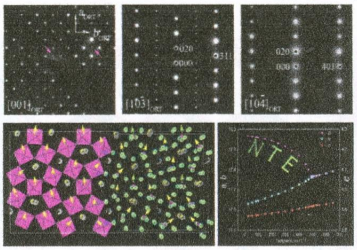

9181 (S) dx.doi.org/10.1021/ic501230m

NHC Copper(I) Complexes Bearing Dipyridylamine Ligands: Synthesis, Structural, and Photoluminescent Studies

Ronan Marion, Fabien Sguerra, Florent Di Meo, Elodie Sauvageot, Jean-François Lohier, Richard Daniellou, Jean-Luc Renaud, Mathieu Linares,* Matthieu Hamel,* and Sylvain Gaillard*

Bright and blue: a series of new tricoordinated cationic copper complexes bearing a NHC and a N^N ligand were synthesized and fully characterized. Thanks to the dipyridylamine ligands, the stressed geometry yields blue photoluminescent material.

9192 (S) dx.doi.org/10.1021/ic501273b

A Structural and Spectroscopic Investigation of Octahedral Platinum Bis(dithiolene)phosphine Complexes: Platinum Dithiolene Internal Redox Chemistry Induced by Phosphine Association

P. Chandrasekaran,* Angelique F. Greene, Karen Lillich, Stephen Capone, Joel T. Mague, Serena DeBeer, and James P. Donahue*

Platinum bis(dithiolene) complexes, prepared via transmetalation with $Me_2Sn(S_2C_2R_2)$, form octahedral adducts with phosphines. Structural characterization by X-ray crystallography shows that the dithiolene ligands are reduced from radical monoanions to ene-1,2-dithiolates to accommodate the IV+ oxidation state typical of six-coordinate platinum. This internal metal–ligand redox change is corroborated by cyclic voltammetry and spectroscopically by UV–vis and S K-edge and Pt L_1-edge XAS. The XAS spectra show reduced sulfur and oxidized platinum for $[Pt(S_2C_2R_2)_2(phosphine)_2]$ relative to $[Pt(S_2C_2R_2)_2]$.

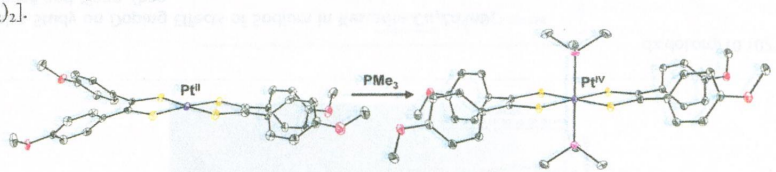

9206 S dx.doi.org/10.1021/ic501271t

Structure, Phase Transition, and Controllable Thermal Expansion Behaviors of $Sc_{2-x}Fe_xMo_3O_{12}$

Meimei Wu,* Xinzhi Liu, Dongfeng Chen,* Qingzhen Huang, Hui Wu, and Yuntao Liu

X-ray and neutron diffraction results indicate that $Sc_{1.3}Fe_{0.7}Mo_3O_{12}$ exhibits near zero thermal expansion, and the volumetric coefficient of thermal expansion derived from X-ray and neutron diffraction is 0.28×10^{-6} °C^{-1} (250–800 °C) and 0.65×10^{-6} °C^{-1} (227–427 °C), respectively. Neutron diffraction results indicate that the bridging angles, Sc(Fe)–Mo nonbond distance, and the volume distortion of $Sc(Fe)O_6$ are closely related to the negative or zero thermal expansion feature in $Sc_2Mo_3O_{12}$ and $Sc_{1.3}Fe_{0.7}Mo_3O_{12}$.

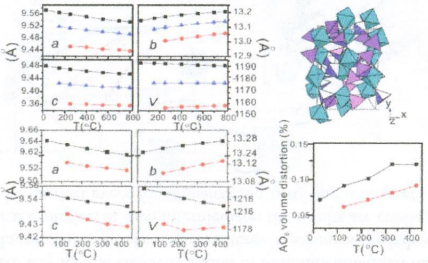

9213 S dx.doi.org/10.1021/ic501313q

Perturbation of the Charge Density between Two Bridged Mo_2 Centers: The Remote Substituent Effects

Tao Cheng, Miao Meng, Hao Lei, and Chun Y. Liu*

A series of six terephthalate-bridged dimolybdenum dimers with various formamidinate ligands has been studied. Substituent effects on electron delocalization between the two $[Mo_2]$ sites are shown by linear correlation of the experimental parameters ($\Delta E_{1/2}$, λ_{max}, and $\Delta\delta_{\parallel-\perp}$) with the Hammett constants (σ_X).

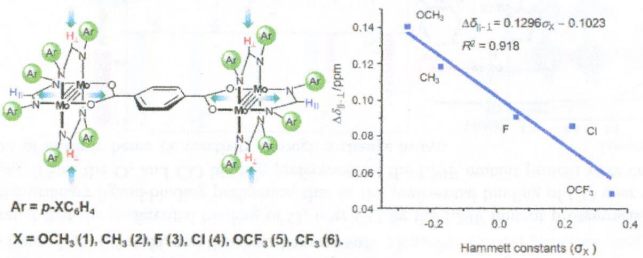

9222 dx.doi.org/10.1021/ic501306n

Crystal Structure and Microwave Dielectric Behaviors of Ultra-Low-Temperature Fired $x(Ag_{0.5}Bi_{0.5})MoO_4-(1-x)BiVO_4$ ($0.0 \leq x \leq 1.0$) Solid Solution with Scheelite Structure

Di Zhou,* Li-Xia Pang, and Ze-Ming Qi

When $x < 0.10$, the ceramic samples crystallized in a monoclinic scheelite structure and a tetragonal scheelite solid solution was formed when $x \geq 0.10$. The $x = 0.10$ sample could be well sintered at 610 °C and possesses high performance of microwave dielectric properties with permittivity ~78 and $Q_f \approx$ 9900 GHz.

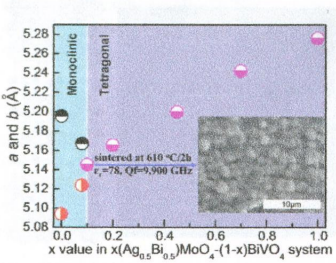

9228 dx.doi.org/10.1021/ic501321z

Hydrothermal Fabrication of $MnCO_3$@rGO Composite as an Anode Material for High-Performance Lithium Ion Batteries

Liankai Zhou, Xianghua Kong,* Min Gao, Fang Lian, Baojun Li, Zhongfu Zhou, and Huaqiang Cao*

$MnCO_3$@rGO (MGC) composite was fabricated through a hydrothermal synthesis of $MnCO_3$ nanoparticles by using L-lysine in the hydrothermal reduction process of graphene oxide to reduced graphene oxide sheets. The MGC was employed as an anode active material for lithium ion batteries. Excellent performances were obtained with a high specific capacity up to 857 $mA{\cdot}h{\cdot}g^{-1}$ after 100 cycles. The enhanced structure stability and ion/electron conductivity of the MGC are responsible for the superior electrochemical properties.

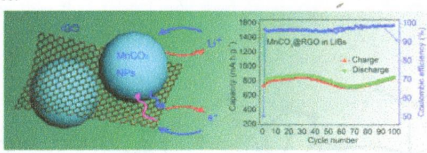

9235 dx.doi.org/10.1021/ic5013268

First-Principles Study on Doping Effects of Sodium in Kesterite Cu_2ZnSnS_4

Zong-Yan Zhao* and Xiang Zhao

For kesterite Cu_2ZnSnS_4, Na doping could reduce the effective mass of holes on the top of the valence band, resulting in the following aspects for CZTS-based thin film solar cell devices: carrier concentration increase, hole mobility enhancement, and minority carrier lifetime elongation. At the same time, the fundamental absorption edge is blue-shifted when Na occupies the cation lattice sites, while it is red-shifted when Na occupies the interstitial sites.

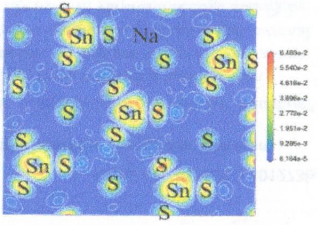

9242 dx.doi.org/10.1021/ic5013389

Synthesis and Reactivity of Tripodal Complexes Containing Pendant Bases

Johanna M. Blacquiere,* Michael L. Pegis, Simone Raugei, Werner Kaminsky, Amélie Forget, Sarah A. Cook, Taketo Taguchi, and James M. Mayer*

A new family of tripodal complexes with basic moieties in the second-coordination sphere, $[M(L)]^-$ (M = Co, Zn), were designed as electrocatalysts for dioxygen reduction. The synthesis and characterization of the ligands and their complexes are presented. The addition of dioxygen yields cobalt(III) superoxo products, observed in minor quantities. The complexes $[M(L)]^-$ are not stable when treated with excess acid, conditions that are typical for electrocatalytic dioxygen reduction.

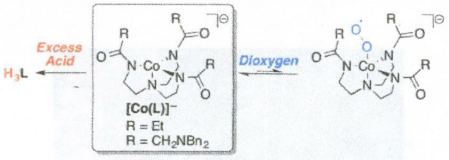

9254 S dx.doi.org/10.1021/ic5013473

Tuning CO_2 Selective Adsorption over N_2 and CH_4 in UiO-67 Analogues through Ligand Functionalization

Bin Wang, Hongliang Huang, Xiu-Liang Lv, Yabo Xie, Ming Li,* and Jian-Rong Li*

Two UiO-67 analogues with carbonyl or sulfone functionalized ligands have been synthesized that show enhanced CO_2 adsorption capacities and selectivities over N_2 and CH_4 compared with UiO-67. This result demonstrates that introducing the two kinds of functional groups into pores of MOFs can significantly increase their affinity toward CO_2 molecules, thereby achieving high CO_2 capture ability.

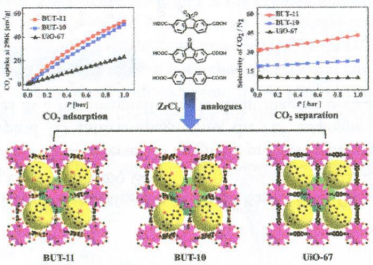

9260 S dx.doi.org/10.1021/ic501364h

van der Waals Radii of Noble Gases

Jürgen Vogt* and Santiago Alvarez*

The analysis of van der Waals contacts involving noble gases in the solid state and in the gas phase furnishes an interatomic distances data set that allows for the extraction of periodically consistent van der Waals radii.

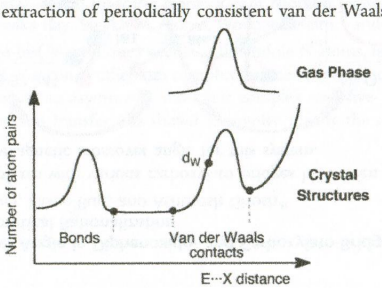

9267 dx.doi.org/10.1021/ic501381v

Novel One-, Two-, and Three-Dimensional Selenidostannates Templated by Iron(II) Complex Cation

Chunying Tang, Fang Wang, Jialin Lu, Dingxian Jia,* Wenqing Jiang, and Yong Zhang

The novel selenidostannates $[Fe(bipy)_3]Sn_4Se_9 \cdot 2H_2O$ (**1**) and $[Fe(bipy)_3]_2[Sn_3Se_7]_2 \cdot bipy \cdot 2H_2O$ (**2**) (bipy = 2,2′-bipyridine) were prepared under hydrothermal conditions. **1** comprises the 3-D framework selenidostannate $^3_\infty[Sn_4Se_9^{2-}]$ with a interpenetrating channel system, in which the $[Fe(bipy)_3]^{2+}$ cations are included. **2** is the first example of a selenidostannate containing both $^1_\infty[Sn_3Se_7^{2-}]$ chainlike and $^2_\infty[Sn_3Se_7^{2-}]$ layered anions.

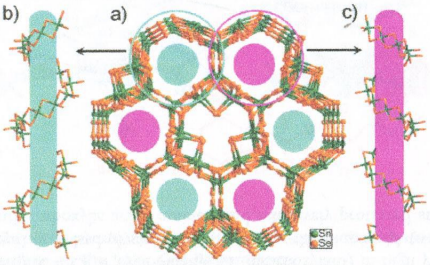

9274 dx.doi.org/10.1021/ic501385r

Synthesis, Detailed Characterization, and Theoretical Understanding of Mononuclear Chromium(III)-Containing Polyoxotungstates $[Cr^{III}(HX^{V}W_7O_{28})_2]^{13-}$ (X = P, As) with Exceptionally Large Magnetic Anisotropy

Wenjing Liu, Jonathan H. Christian, Rami Al-Oweini, Bassem S. Bassil, Johan van Tol, Mihail Atanasov,* Frank Neese,* Naresh S. Dalal,* and Ulrich Kortz*

We have prepared the first two mononuclear chromium-substituted heteropolytungstates $[Cr^{III}(HP^{V}W_{28})_2]^{13-}$ (**1a**) and $[Cr^{III}(HAs^{V}W_7O_{28})_2]^{13-}$ (**2a**) via a simple, one-pot procedure. Polyanions **1a** and **2a** comprise an octahedrally coordinated Cr^{III} ion, sandwiched by two $\{PW_7\}$ or $\{AsW_7\}$ units. Magnetic studies demonstrated that both compounds deviate from typical paramagnetic behavior, with an exceptionally large zero-field uniaxial anisotropy parameter, $D = +2.4\ cm^{-1}$, the largest and sign-assigned D-value so far reported for a Cr^{III}-containing molecular compound.

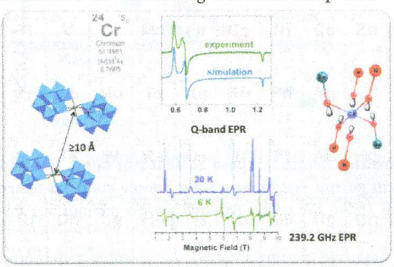

9284 Ⓢ dx.doi.org/10.1021/ic5013999

Synthesis, Structure, and Catalytic Applications for *ortho*- and *meta*-Carboranyl Based NBN Pincer-Pd Complexes

Min Ying Tsang, Clara Viñas, Francesc Teixidor, José Giner Planas,* Nerea Conde, Raul SanMartin, María Teresa Herrero, Esther Domínguez, Agustí Lledós, Pietro Vidossich, and Duane Choquesillo-Lazarte

Synthesis and structural studies of *o*- and *m*-carborane-based NBN pincer palladium complexes are described, along with density functional theory calculations conducted to gain more insight into these new carboryl motifs. Catalytic applications of **(*o*CB-L1)Pd** and **(*m*CB-L1)Pd** have shown the complexes are good catalyst precursors in Suzuki coupling in water and with remarkably low amounts of catalyst loadings.

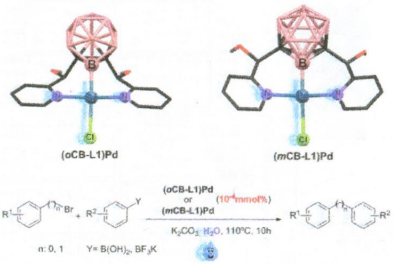

9296 Ⓢ dx.doi.org/10.1021/ic501425x

Ferro- to Antiferromagnetic Crossover Angle in Diphenoxido- and Carboxylato-Bridged Trinuclear Ni^{II}_2–Mn^{II} Complexes: Experimental Observations and Theoretical Rationalization

Piya Seth, Albert Figuerola,* Jesús Jover, Eliseo Ruiz, and Ashutosh Ghosh*

Three new trinuclear Ni^{II}–Mn^{II} complexes with various carboxylato bridges have been synthesized and characterized to explore the antiferromagnetic to ferromagnetic crossover angle for this system.

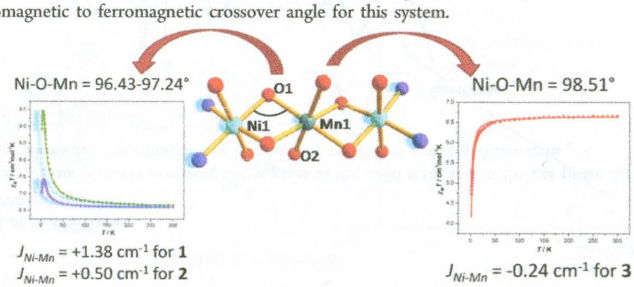

$J_{Ni\text{-}Mn}$ = +1.38 cm^{-1} for **1**
$J_{Ni\text{-}Mn}$ = +0.50 cm^{-1} for **2**
$J_{Ni\text{-}Mn}$ = -0.24 cm^{-1} for **3**

9306 Ⓢ dx.doi.org/10.1021/ic5014279

Magnetic Coupling and Slow Relaxation of Magnetization in Chain-Based Mn^{II}, Co^{II}, and Ni^{II} Coordination Frameworks

Jian-Yong Zhang, Kun Wang, Xiu-Bing Li, and En-Qing Gao*

Three isomorphous coordination networks show diverse 1D magnetic properties because of the chain with $(\mu\text{-COO})_2(\mu\text{-}N_3)$ bridges: the Mn^{II} compound shows typical 1D antiferromagnetism, the Ni^{II} analogue shows 1D ferromagnetism and slow relaxation, and the Co^{II} species behaves as a ferromagnetic single-chain magnet because of Glauber dynamics.

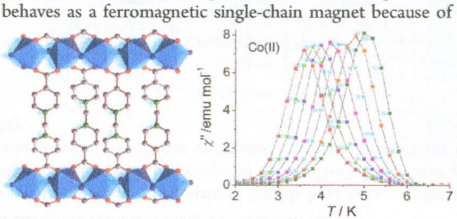

9315 S dx.doi.org/10.1021/ic501438k

Potential of Cycloaddition Reactions To Generate Cytotoxic Metal Drugs In Vitro

Benjamin S. Murray,* Stéphanie Crot, Sviatlana Siankevich, and Paul J. Dyson*

The strain-promoted cycloaddition between a Ru^{II} organometallic compound, functionalized at the arene ligand with a bicyclononyne derivative, and a ditetrazine yields the formation of a dinuclear organometallic compound in biological media. The dinuclear compound exhibits increased cytotoxicity against tumorigenic cells relative to its constituent components, yielding a novel route toward their cytotoxic activation in cellulo.

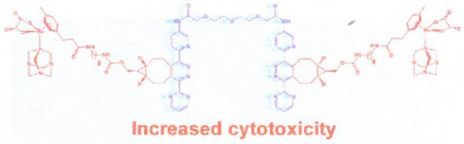

9322 dx.doi.org/10.1021/ic501442g

Thermodynamic Consistencies and Anomalies among End-Member Silicate Garnets

Leslie Glasser*

There exist much experimental data for the mineral silicate garnets, which are highly ionic solids. Using earlier-developed methods, we examine the thermodynamic relations among these structurally related materials and note some useful consistencies. We develop additive single-ion values that may be used to estimate formation enthalpies for silicate garnets and related materials.

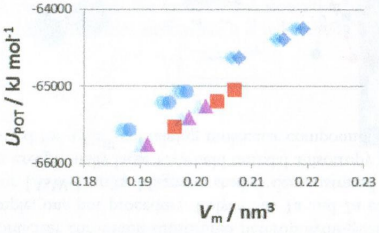

9326 S dx.doi.org/10.1021/ic501446b

A New Entry to Asymmetric Platinum(IV) Complexes via Oxidative Chlorination

Mauro Ravera, Elisabetta Gabano, Giorgio Pelosi, Federico Fregonese, Stefano Tinello, and Domenico Osella*

The oxidative chlorination of diam(m)inodichlorido or diam(m)inodicarboxylato Pt(II) compounds in ethane-1,2-diol with *N*-chlorosuccinimide was used to produce asymmetric Pt(IV) complexes $[PtA_2Cl(glyc)X_2]$ (A = NH_3 or cyclohexane-1*R*,2*R*-diamine; glyc = 2-hydroxyethanolato; X = Cl or cyclobutane-1,1′-dicarboxylato) in high yield and purity. The trichlorido complexes easily undergo a pH-dependent hydrolysis reaction, whereas the dicarboxylato compounds are stable enough to allow further coupling reactions with carboxylic acids, amines, and selectively protected amino acids via the glyc reactive pendant.

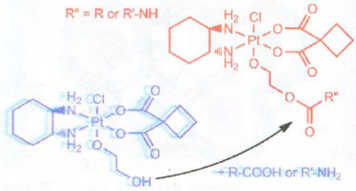

9336 dx.doi.org/10.1021/ic5014544

Redox and Photoinduced Electron-Transfer Properties in Short Distance Organoboryl Ferrocene-Subphthalocyanine Dyads

Eranda Maligaspe, Matthew R. Hauwiller, Yuriy V. Zatsikha, Jonathan A. Hinke, Pavlo V. Solntsev, David A. Blank,* and Victor N. Nemykin*

Two new ferrocenyl-subphthalocyanine dyads with ferrocene (**2**) and ethynylferrocenyl (**3**) substituents directly attached to the subphthalocyanine ligand via axial position have been prepared and characterized using NMR, UV−vis, and magnetic circular dichroism (MCD) spectroscopies, electrochemistry, and X-ray crystallography. The electronic structures and the nature of the optical bands observed in the UV−vis and MCD spectra of all target compounds were investigated by density functional theory-polarized continuum model (DFT-PCM) and time-dependent (TDDFT-PCM) approaches. Time resolved pump−probe spectroscopy was used to quantify the rates of both charge separation and charge recombination in new dyads **2** and **3** and were compared to those in ferrocenyl-subphthalocyanine dyads with ferrocenemethoxide (**4**) and ferrocene carboxylate (**5**) substituents attached to the subphthalocyanine ligand via axial position.

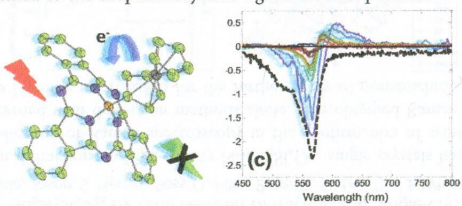

9348 dx.doi.org/10.1021/ic501460d

Uncommon *cis* Configuration of a Metal−Metal Bridging Noninnocent Nindigo Ligand

Prasenjit Mondal, Sebastian Plebst, Ritwika Ray, Shaikh M. Mobin, Wolfgang Kaim,* and Goutam Kumar Lahiri*

Coordination of $[Ru(bpy)_2]^{2+}$ to indigo-bis(*N*-arylimine) occurs at the indole N atoms, leading to a *cis* configuration of the central C−C bond. A second ruthenium complex fragment, $[Ru(acac)_2]$, could be chelated by the imine N atoms, leading to an asymmetric dinuclear complex with five- and seven-membered ring chelation. Multiple-electron transfer was shown to involve mainly the redox-active bridge.

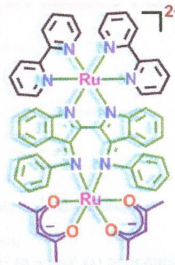

9357 dx.doi.org/10.1021/ic501465v

Preparation and Hydrosilylation Activity of a Molybdenum Carbonyl Complex That Features a Pentadentate Bis(imino) pyridine Ligand

Raja Pal, Thomas L. Groy, Amanda C. Bowman, and Ryan J. Trovitch*

While refluxing ^{PyEt}PDI and $Mo(CO)_6$ resulted in the formation of $(^{PyEt}PDI)_2Mo$, conducting the same reaction with ^{Ph2PPr}PDI afforded $(^{Ph2PPr}PDI)Mo(CO)$. Both complexes were found to catalyze benzaldehyde hydrosilylation at 90 °C, and the optimization of $(^{Ph2PPr}PDI)Mo(CO)$-mediated aldehyde hydrosilylation resulted in turnover frequencies of up to 330 h^{-1}. Utilizing single-crystal X-ray diffraction, DFT analysis, and cyclic voltammetry, both complexes were found to possess neutral bis(imino)pyridine chelates that accept Mo-based electron density through π-back-bonding.

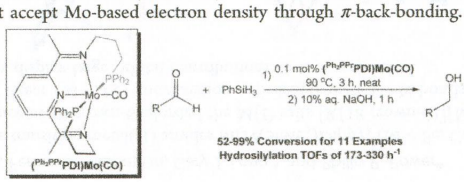

9366 dx.doi.org/10.1021/ic501474r

Os(II) Phosphors with Near-Infrared Emission Induced by Ligand-to-Ligand Charge Transfer Transition

Jia-Ling Liao, Yun Chi,* Shih-Hung Liu, Gene-Hsiang Lee, Pi-Tai Chou,* Hao-Xiang Huang, Yu-De Su, Chih-Hao Chang,* Jin-Sheng Lin, and Meu-Rurng Tseng*

A contour plot of the electronic transition from ground state (blue) to the lowest energy triplet excited state (pink) of **3**, showing the metal-to-ligand charge transfer contribution at the lowest electronically excited state.

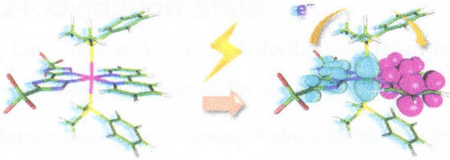

9375 dx.doi.org/10.1021/ic501479p

Novel Ruthenium Sensitizers Having Different Numbers of Carboxyl Groups for Dye-Sensitized Solar Cells: Effects of the Adsorption Manner at the TiO_2 Surface on the Solar Cell Performance

Hironobu Ozawa, Takahito Sugiura, Ryosuke Shimizu, and Hironori Arakawa*

A novel ruthenium sensitizer having multiple carboxyl groups (**TUS-21**) has been synthesized for dye-sensitized solar cells (DSCs). **TUS-21** binds to the TiO_2 surface by using two carboxyl groups at the 3-position of the phenyl ring and at one of the terminal pyridine rings of the terpyridine ligand. The DSC with **TUS-21** exhibited 10.2% conversion efficiency under AM 1.5 (100 mW/cm^2) irradiation.

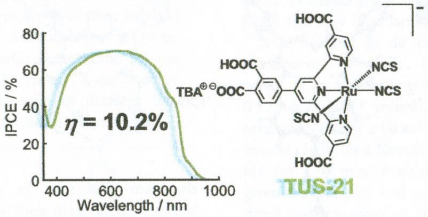

9385 dx.doi.org/10.1021/ic501526g

Carba-*closo*-dodecaborate Anions with Two Functional Groups: [1-R-12-HC≡C-*closo*-1-$CB_{11}H_{10}$]$^-$ (R = CN, NC, CO_2H, C(O)NH_2, NHC(O)H)

Michael Hailmann, Szymon Z. Konieczka, Alexander Himmelspach, Jochen Löblein, Guido J. Reiss, and Maik Finze*

Syntheses of salts of new difunctionalized carba-*closo*-dodecaborate anions with one functional group bonded to the cluster C atom and an ethynyl group attached to the antipodal boron atom were developed. The $[Et_4N]^+$ salts of the five anions were characterized. Furthermore, the transmission of electronic effects through the {*closo*-1-CB_{11}} cage was proven by a combined experimental-theoretical study based on ^{13}C NMR spectroscopic data. Additionally, the first syntheses of salts of the isocyano derivative [1-CN-*closo*-1-$CB_{11}H_{11}$]$^-$ are described.

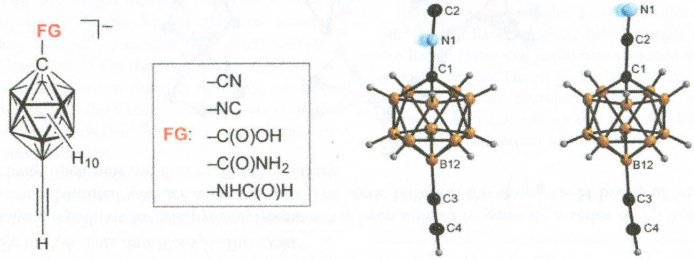

9400 S dx.doi.org/10.1021/ic501534f

Synthesis, Structure, and Magnetic and Electrochemical Properties of Quasi-Linear and Linear Iron(I), Cobalt(I), and Nickel(I) Amido Complexes

Chun-Yi Lin, James C. Fettinger, Fernande Grandjean, Gary J. Long,* and Philip P. Power*

Reduction of the two-coordinate transition metal(II) amides $M[N(SiMe_3)Dipp\}_2$ (M = Fe, Co, N; Dipp = C_6H_3-2,6-Pr^i_2) with potassium graphite in the presence of 18-crown-6 afforded the M(I) salts $[K(18\text{-crown-}6)][M\{N(SiMe_3)Dipp\}_2]$, which have linear (M = Co, Ni) or almost linear (M = Fe) coordination with lengthened M–N bonds. Magnetic studies showed the iron(I) and cobalt(I) complexes display large orbital contributions to their moments.

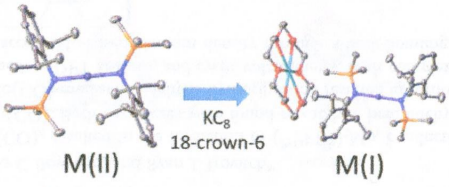

9407 S dx.doi.org/10.1021/ic5015412

Cation Ordering and Flexibility of the BO_4^{2-} Tetrahedra in Incommensurately Modulated $CaEu_2(BO_4)_4$ (B = Mo, W) Scheelites

Artem M. Abakumov,* Vladimir A. Morozov, Alexander A. Tsirlin, Johan Verbeeck, and Joke Hadermann

Flexible BO_4^{2-} (B = Mo, W) tetrahedra mediate interactions behind the A-site cation ordering in the $(A',A'')_{1-x}BO_4$ scheelites. The structure map of the $(A',A'')_{1-x}BO_4$ scheelites demonstrates dependence of the A-site cation ordering on the difference in the ionic radii of the A-cations $r(A') - r(A'')$ and the fraction of the cation vacancies x.

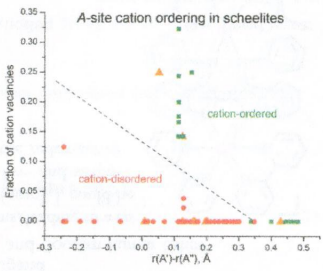

9416 S dx.doi.org/10.1021/ic501558r

Structural Study of the Apatite $Nd_8Sr_2Si_6O_{26}$ by Laue Neutron Diffraction and Single-Crystal Raman Spectroscopy

Tao An,* Alodia Orera, Tom Baikie, Jason S. Herrin, Ross O. Piltz, Peter R. Slater, Tim J. White, and María L. Sanjuán*

A full Raman study and neutron diffraction on high-quality $Nd_8Sr_2Si_6O_{26}$ single crystals have been performed for structural solution, demonstrating the application of Raman spectroscopy in the confirmation of symmetry between $P6_3$ and $P6_3/m$, which are too similar to be discerned with diffraction methods alone. The obtained Raman spectra from this stoichiometric composition could thus serve as baseline information for the further study of nonstoichiometry apatite compounds.

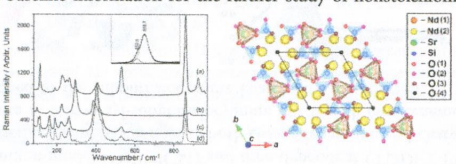

9424 Ⓢ dx.doi.org/10.1021/ic5015658

Ferrocenyl-Substituted Tris(pyrazolyl)borates—A New Ligand Type Combining Redox Activity with Resistance to Hydrogen Atom Abstraction

Eric R. Sirianni, Glenn P. A. Yap, and Klaus H. Theopold*

A Lewis acid catalyzed synthesis for tris(pyrazolyl)borates has been utilized to generate a series of Tp ligands in which all pyrazolyl groups are substituted with ferrocenyl groups. The steric bulk and the strong C–H bonds of ferrocene combined with its redox activity open new avenues in TpM chemistry.

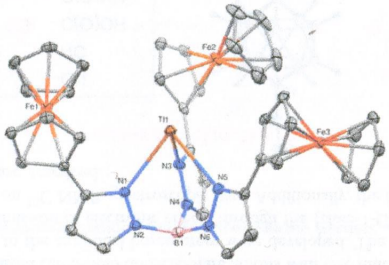

9431 Ⓢ dx.doi.org/10.1021/ic501629n

Phosphorus Complexes of *meso*-Triaryl-25-oxasmaragdyrins

Hemanta Kalita, Way-Zen Lee, and Mangalampalli Ravikanth*

The syntheses, structure, and spectral and electrochemical properties of PO_2 complexes of smaragdyrins are described.

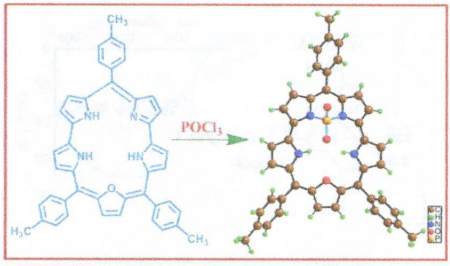

Additions and Corrections

9439 dx.doi.org/10.1021/ic501173a

Correction to Single-Crystal Growth and Size Control of Three Novel Polar Intermetallics: $Eu_{2.94(2)}Ca_{6.06}In_8Ge_8$, $Eu_{3.13(2)}Ca_{5.87}In_8Ge_8$, and $Sr_{3.23(3)}Ca_{5.77}In_8Ge_8$ with Crystal Structure, Chemical Bonding, and Magnetism Studies

Hyein Woo, Gnu Nam, Eunyoung Jang, Jin Kim, Yunho Lee, Kyunghan Ahn, Svilen Bobev, and Tae-Soo You*

Ⓢ Supporting Information available via online article